A&A 423, 1081–1094 (2004)
DOI: 10.1051/0004-6361:20040355

Astronomy & Astrophysics

Discovery of kilogauss magnetic fields in three DA white dwarfs⋆

R. Aznar Cuadrado[1], S. Jordan[2,3], R. Napiwotzki[4], H. M. Schmid[5], S. K. Solanki[1], and G. Mathys[6]

[1] Max-Planck-Institut für Aeronomie, Max-Planck-Str. 2, 37191 Katlenburg-Lindau, Germany
e-mail: aznar@linmpi.mpg.de
[2] Institut für Astronomie und Astrophysik, Eberhard-Karls-Universität Tübingen, Sand 1, 72076 Tübingen, Germany
[3] Astronomisches Rechen-Institut, Mönchhofstr. 12–14, 69120 Heidelberg, Germany
[4] Department of Physics & Astronomy, University of Leicester, University Road, Leicester LE1 7RH, UK
[5] Institut für Astronomie, ETH Zentrum, 8092 Zürich, Switzerland
[6] European Southern Observatory, Casilla 19001, Santiago 19, Chile

Received 27 February 2004 / Accepted 12 May 2004

Abstract. We have detected longitudinal magnetic fields between 2 and 4 kG in three (WD 0446−790, WD 1105−048, WD 2359−434) out of a sample of 12 normal DA white dwarfs by using optical spectropolarimetry done with the VLT Antu 8 m telescope equipped with FORS1. With the exception of 40 Eri B (4 kG) these are the first positive detections of magnetic fields in white dwarfs below 30 kG. Although suspected, it was not clear whether a significant fraction of white dwarfs contain magnetic fields at this level. These fields may be explained as relics from magnetic fields in the main-sequence progenitors considerably enhanced by magnetic flux conservation during the shrinkage of the core. A detection rate of 25% (3/12) may indicate now for the first time that a substantial fraction of white dwarfs have a weak magnetic field. This result, if confirmed by future observations, would form a cornerstone for our understanding of the evolution of stellar magnetic fields.

Key words. stars: magnetic fields – stars: individual: WD0446-790, WD1105-048, WD2359-434

1. Introduction

The major goal of this work is a better understanding of the role played by magnetic fields in the formation and evolution of stars. Magnetic fields are already an important ingredient during the collapse and fragmentation of protostellar clouds which ultimately determines the initial field of pre-main sequence stars. On the main sequence and at later stages of evolution the magnetic fields have a major impact on the angular momentum loss and stellar winds, on building-up chemical anomalies and abundance inhomogeneities across the stellar surface, on convection and the related coronal activity, and other evolutionary processes especially in interacting binaries. Very strong magnetic fields are detected in several white dwarfs and are always present in pulsars (Mestel 2001). The first detection of a magnetic field on a white dwarf was made by Kemp et al. (1970) on Grw+70° 8247, and large spectroscopic and polarimetric surveys have been carried out in the last two decades (e.g. Hagen et al. 1987; Reimers et al. 1994; Schmidt & Smith 1995; Putney 1995; Kawka et al. 2003). For the white dwarfs the magnetic fields could simply be "fossil" remnants of the fields already present in main-sequence stars, but strongly amplified by contraction. This hypothesis assumes that the magnetic flux (e.g. through the magnetic equator) is conserved to a large extent during the stellar evolution.

According to the field amplification theory, the white dwarfs play an important role in the investigation of stellar magnetic fields. In main-sequence stars magnetic fields have been detected directly mainly for peculiar magnetic Ap and Bp stars with rather well organized fields and field strengths of the order 10^2–10^4 Gauss. For weak fields in A to O stars ($B < 10^2$ G) direct magnetic field detections are still very rare (e.g. the field detections in early B stars reported by Neiner et al. 2003a,b). For sun-like stars ample evidence (coronal activity) for the presence of complicated small-scale fields exists, but direct measurements are only possible for the more active stars (Saar 1996; Rüedi et al. 1997; Valenti & Johns-Krull 2001). The contraction to a white dwarf amplifies the magnetic fields by about 4 orders of magnitude, so that weak and often undetectable magnetic fields on the main sequence become measurable during the white dwarf phase. This is supported by the known magnetic white dwarfs with megagauss fields ($B = 10^6$–10^9 G). Their frequency and space distribution, as well as their mass, are consistent with the widely accepted view that they are the descendents of the magnetic Ap and Bp stars (e.g. Mathys 2001). Another origin seems to be required for the magnetic degenerates with weaker fields (unless magnetic flux is lost during the contraction phase). Magnetic main-sequence stars with weaker magnetic fields have been

⋆ Based on observations collected at the European Southern Observatory, Paranal, Chile, under programme ID 70.D-0259.

suggested as their possible progenitor candidates (Schmidt et al. 2003; Kawka et al. 2003). The B stars on which weaker fields have been detected may be the missing stars. However, even the most sensitive observations are limited to some tens of gauss on main-sequence stars.

Thus, magnetic field amplification during stellar evolution may offer the opportunity to investigate ∼1 G magnetic fields (averaged global fields) in normal main-sequence stars with observations of ∼1 kG magnetic fields during the white dwarf stage. White dwarfs with magnetic fields below 100 kG have been either found by searching for circular polarization (Schmidt & Smith 1994) or by looking for Zeeman splitting of narrow NLTE line cores in the Balmer lines, particularly in Hα (Koester et al. 1998). However, the splitting becomes undetectable in intensity spectra for weak fields (<20 kG) or for objects without narrow line core. Therefore, spectropolarimetry is the most promising technique for successful detections of weak magnetic fields. Up to now detections of magnetic fields below 30 kG have not been achieved, except for the very bright white dwarf 40 Eri B (V = 8.5), in which Fabrika et al. (2003) have detected a magnetic field as low as 4 kG. The magnetic field detection limit can now be pushed down to a few kG for many white dwarfs with spectropolarimetry using 8–10 m class telescopes.

In this paper we present and analyse VLT spectropolarimetric data of a sample of 12 white dwarfs in a search for weak magnetic fields. In Sect. 2 the observations and data reduction are described, while in Sect. 3 the observational method for obtaining the Stokes parameter (V/I) is described. Section 4 presents the method for determining weak magnetic fields analysing the circular polarisation due to a given magnetic field. In that section we also present the results of our analysis, along with the description of the χ^2-minimisation procedure applied to our data. The determination of the atmospheric and stellar parameters is presented in Sect. 5 and compared with those found in the literature. A discussion and conclusions are presented in Sect. 6.

2. Observations and data reduction

Spectropolarimetric observations of a sample of 12 normal DA white dwarfs were carried out during the period 4 November 2002–3 March 2003, in service mode by ESO staff members using FORS1 at the 8 m Unit Telescope 1 (UT1) of the Very Large Telescope, "Antu". FORS1 is a multi-mode focal reducer imager and grism spectrograph equipped with a Wollaston prism and rotatable retarder plate mosaics in the parallel beam allowing linear and circular polarimetry and spectropolarimetry (Appenzeller et al. 1998).

With a 0.8″ wide slit we obtained a (FWHM) spectral resolution of 4.5 Å. The data were recorded with a backside-illuminated thinned, AR coated Tek. 2048 × 2048 CCD with 24 μm pixels which correspond to a pixel scale of 0.2″/pixel in spatial and 1 Å/pixel in spectral direction.

Spectra were acquired with grism G600B, which allows observations in the spectral range 3400–6000 Å, covering all H I Balmer lines from Hβ to the Balmer jump simultaneously. A reflex image from the FORS optics affects the wavelength region from 4000 to 4100 Å which corresponds to the blue wing of the Hδ line. Although the reflex shows up in the intensity spectrum it seems to produce no spurious signal in circular polarisation. The reflex is known to occur for this particular grism G600B / Wollaston configuration (e.g. Schmid et al. 2003).

The observations were split into several cycles to avoid saturation. The feasibility of circular spectropolarimetry with the required high signal-to-noise ratio using FORS1 had been demonstrated by Bagnulo et al. (2002, 2004) with test measurements of one magnetic and one non-magnetic A-star. Stellar rotation may cause continuous changes in the field orientation and, therefore, in the polarisation signal. Hence, we have split the observations of an individual target into more than one polarisation measurement taken during different nights (see Sect. 3). In this way, there is a much lower probability that a candidate with a magnetic field escapes detection due to a special orientation at the time of the observations (where circular polarisation cancels). Hence, having for most objects data for more than one epoch, we are able to assess the presence of rotational modulation of a possible magnetic field.

2.1. Selection of the sample

We have searched for the circular polarisation signatures of the Zeeman effect in the Balmer lines in 12 of the brightest southern white dwarfs (having 11.4 mag < V < 14 mag) with RA between 0^h and 12^h.

Our sample was carefully selected on the basis of VLT-UVES spectra taken within the SPY survey (Napiwotzki et al. 2003): SPY (**S**upernovae type Ia **P**rogenitor surve**Y**) is a radial velocity search for close binary systems of two white dwarfs (double degenerates; DD). If these systems are close enough they will merge due to gravitational wave radiation and if the combined mass of these mergers exceed the Chandrasekhar limit for white dwarfs these are potential progenitors of Supernovae type Ia.

SPY was carried out with the high-resolution Echelle spectrograph UVES at the Kueyen (UT2) of VLT. With the set-up used for SPY UVES provides almost complete spectral coverage of the wavelength range from 3200 Å to 6650 Å, with a spectral resolution of 0.3 Å. For more details, please refer to Napiwotzki et al. (2001, 2003). SPY observations were used to check candidates for our project for spectral peculiarities and magnetic fields strong enough to be detected in intensity spectra. Hence, our targets were selected with the criterion of not having any sign of Zeeman splitting visible in the SPY spectra, and hence no magnetic fields above a level of about 20 kG.

All our targets have strong hydrogen lines, ideal for measuring line polarisation, and no peculiarities (such as MG-magnetic fields or a bright companion or any indication of magnetic fields).

2.2. Data reduction

Data reduction was performed using MIDAS routines. Flat field, bias and wavelength calibration exposures were taken during

Table 1. Details of VLT observations. The provided α and δ coordinates refer to epoch 2000 as measured in the course of the SPY project (see Koester et al. 2001). Spectral types, T_{sp}, and measured V magnitudes were taken from the catalogue of McCook & Sion (1999).

Target	Alias	α	δ	V (mag)	HJD (+2 452 500)	t_{exp} (s)	n	T_{sp}
WD 0135−052	LHS 1270	01 37 59.4	−04 59 45	12.84	108.584	546	4	DA7
WD 0227+050	Feige 22	02 30 16.6	+05 15 51	12.65	137.601	381	6	DA3
					169.545	381	6	
WD 0310−688	CPD−69 177	03 10 31.0	−68 36 03	11.40	195.536	119	14	DA3
WD 0346−011	GD 50	03 48 50.2	−00 58 31	13.99	137.657	699	4	DA1
					174.600	699	4	
WD 0446−789	BPM 03523	04 43 46.4	−78 51 50	13.47	109.710	699	4	DA3
					168.569	699	4	
WD 0612+177	LTT 11818	06 15 19.0	+17 43 48	13.39	109.756	699	4	DA2
					172.561	699	4	
WD 0631+107	KPD0631+1043	06 33 50.6	+10 41 09	13.82	200.612	699	4	DA2
					202.607	699	4	
WD 0839−327	CD−32 5613	08 41 32.6	−32 56 35	11.90	108.803	186	10	DA6
WD 0859−039	RE 0902-040	09 02 17.3	−04 07 12	12.40	174.709	289	8	DA2
					196.701	289	8	
WD 1042−690	BPM 06502	10 44 10.5	−69 18 20	13.09	168.832	426	6	DA3
					174.755	426	6	
					195.783	426	6	
WD 1105−048	LP 672−001	11 08 00.0	−05 09 26	12.92	141.838	486	4	DA3
					169.791	486	4	
WD 2359−434	L 362−81	00 02 10.7	−43 09 55	13.05	83.510	546	4	DA5
					108.542	546	4	

day time with the same instrument setup, after each observing night.

In all frames the bias level was subtracted and the frames were cleaned of cosmic ray hits. For each observing night a unique master flat-field was calculated from the median flux of all flat-fields taken that night. The stellar spectra were extracted from the flat-field corrected frames as a sum over about forty CCD rows for each beam. Sky spectra were obtained from adjacent regions (about twenty CCD rows) on the detector to the observed stars (below and above) and subtracted from the object spectra. Wavelength calibration was done using HgCd, He and Ar arc spectra, which was independently performed for wavelengths of the ordinary and extra-ordinary beams with the corresponding beams of a reference spectrum.

Stokes I was obtained as a sum over all beams, while the calculation of Stokes (V/I) is described in the following section.

3. Circular polarisation

In order to obtain circular polarisation spectra a Wollaston prism and a quarter-wave plate were inserted into the optical path. Each exposure yields two spectra on the detector, one from the extra-ordinary beam and the other from the ordinary beam.

In the ideal case, the polarisation information (one Stokes parameter per exposure) is contained in the ratio, at each wavelength, of the intensities in the two spectra (from the ordinary and extra-ordinary beams) but it is mixed up with the system gain ratio for the pixels concerned. Alternatively, the effect of the not well defined pixel gain can be significantly reduced by inverting the sign of the polarisation effects in a second exposure (by rotating the $\lambda/4$-plate by 90°), while leaving the gain ratios identical (Tinbergen & Rutten 1997). Hence, Stokes V is obtained from a differential measurement of photon counts in either the ordinary or extra-ordinary beams, measured at two different angles of the retarder waveplate. In this way errors from changes in the sky transparency, atmospheric scintillation, and various instrumental effects are significantly reduced, so that photon noise remains as the dominant error source.

Another important source of sytematic error when obtaining Stokes V could be the wavelength calibration procedure. An incorrect calibrated wavelength scale for each of the two analysed spectra will yield the line profiles of the two spectra not perfectly aligned, even in the absence of a magnetic field, leading to spurious polarization signals in each line, that change sign as the wave plate rotates. No such spurious signals were detected during the calibration process, confirming that FORS is a very stable instrument. Even if spurious line signals at the noise level are present, they would be compensated for at least partly by the combination of data taken with retarder plate position angles +45° and −45°. We note that wavelength calibrations were made for each observing date separately. Because most targets were observed for two different dates we could check that no spurious magnetic field detection due to wavelength calibration errors are present.

We adopted the FORS1 standard observing sequence for circular polarimetry consisting of exposures with retarder plate position angles +45° and −45°. The number of exposures, n, is reported in Table 1 for each object. For instance, for $n = 4$ the sequence of position angles would go: +45°, +45°, −45°, −45°.

In order to derive the circular polarisation from a sequence of exposures, we added up the exposures with the same quarter-wave plate position angle. The Stokes (V/I) can be obtained as

$$\frac{V}{I} = \frac{(R-1)}{(R+1)}, \quad \text{with } R^2 = \left(\frac{f_o}{f_e}\right)_{\alpha=+45} \times \left(\frac{f_e}{f_o}\right)_{\alpha=-45} \tag{1}$$

where V is the Stokes parameter which describes the net circular polarisation, I is the unpolarized intensity, α indicates the nominal value of the position angle of the retarder waveplate, and f_o and f_e are the fluxes on the detector from the ordinary and extra-ordinary beams of the Wollaston, respectively. Equation (1) is equivalent to formula 4.1 in the FORS 1+2 User Manual (Szeifert & Böhnhardt 2003). In Donati et al. (1997) a detailed description of the method for the suppression of spurious signals in spectropolarimetric observations that we applied is provided.

The 12 selected white dwarfs are listed in Table 1 together with some characteristics of the observations. The Heliocentric Julian Dates correspond to the beginning of each observing sequence.

4. Determination of weak magnetic fields

4.1. Theoretical polarisation

For the weak magnetic fields expected in our white dwarfs the longitudinal Zeeman effect (due to magnetic fields parallel to the line of sight) is measurable for the broad Balmer lines with intermediate spectral resolution. This is possible because, in a first approximation, the positive and negative extrema of Stokes V occur at the wavelengths where the second derivative of Stokes I changes its sign. These points could possibly be regarded as the transitions between the core and the wings of the line. Hence, the wavelength difference between the maxima of the opposite net circular polarisation in the two wings of the line, is correlated with the width of the core of the line and not with the Zeeman splitting $\Delta\lambda_B$, which can be much smaller. The detection threshold therefore depends mainly on the noise level in V and the width of the core of the spectral lines, and far less on the achieved spectral resolution.

With FORS1 on the VLT we reach a noise level in circular spectropolarimetry of about $3 \times 10^{-3} I_c$, where I_c is the continuum intensity. This allows us to detect magnetic fields of a few kG for the brightest white dwarfs in our sample with exposure times of about 1 h. This is a significant improvement compared to the observations of Schmidt & Smith (1995), who reached a detection limit of about 20 kG (2.3σ limit) with a 2 m class telescope. By adding the signal of several Balmer lines, which are observed simultaneously with our instrument setup, the magnetic sensitivity can be further enhanced. However, the error of the magnetic field determination increases for the higher series numbers, so that a reliable analysis can be based on Hβ and Hγ only.

The theory of spectral line formation in a magnetic atmosphere shows that the splitting of a spectral line observed in both senses of circular polarisation is proportional to $\langle B_z \rangle$, the average of the component of the magnetic field along the line of sight averaged over the visible stellar hemisphere, i.e., the mean longitudinal magnetic field (Babcock 1947, 1958).

For field strengths below 10 kG the Zeeman splitting of the Balmer lines is less than approximately 0.1 Å. This is well below the width of the cores of the Balmer lines in all the stars of our sample (typically a few Å). Therefore, we can apply the weak-field approximation (e.g., Angel & Landstreet 1970; Landi degl'Innocenti & Landi degl'Innocenti 1973) without any loss of accuracy. According to this approximation the measured V and I profiles are related to $\langle B_z \rangle$ by the expression:

$$\frac{V}{I} = -g_{\rm eff} C_z \lambda^2 \frac{1}{I}\frac{\partial I}{\partial \lambda}\langle B_z \rangle, \tag{2}$$

where $g_{\rm eff}$ is the effective Landé factor (=1 for all hydrogen lines of any series, Casini & Landi degl'Innocenti 1994), λ is the wavelength expressed in Å, $\langle B_z \rangle$ is the mean longitudinal component of the magnetic field expressed in Gauss and the constant $C_z = e/(4\pi m_e c^2) (\simeq 4.67 \times 10^{-13}\,\mathrm{G^{-1}\,\AA^{-1}})$. Note that this approximation also holds if instrumental broadening is present, but it is not generally correct if the profiles are rotationally broadened (Landstreet 1982).

Equation (2) is evaluated by using the high signal-to-noise spectra $I(\lambda)$ and their derivative $\partial I/\partial\lambda$. For a given wavelength λ_i we approximate $\partial I/\partial\lambda$ by the average of $(I_{i+1} - I_i)/(\lambda_{i+1} - \lambda_i)$ and $(I_i - I_{i-1})/(\lambda_i - \lambda_{i-1})$.

The error associated with the determination of the longitudinal field obtained from individual Balmer lines is larger for Balmer lines at shorter wavelengths than for lines at longer wavelengths. This is due to the combination of two effects: while the Zeeman effect increases as lambda squared, most other line broadening effects depend linearly on lambda, so that the magnetic field is better detected at longer wavelengths than at shorter wavelengths; furthermore, the Balmer lines at shorter wavelengths are less deep, so that $\partial I/\partial\lambda$ is smaller. Using Hβ and Hγ simultaneously, we obtained a determination of the mean longitudinal magnetic field that best fit the observed (V/I) (as explained in the next section).

4.2. Fitting of the magnetic field

In Fig. 1 we present the normalised spectra of our sample of 12 DA white dwarfs. Multiple observations of the same star were added to achieve a higher signal-to-noise level. In some spectra, particularly prominent in WD 0135-052, a small bump is visible on the blue side of the Hδ line, due to the reflex mentioned in Sect. 2.

For the circular polarisation spectra (V/I) flux weighted means were calculated according to the following formula for two measurements 1 and 2:

$$\left(\frac{V}{I}\right)_{\rm tot} = \frac{\left(\frac{V}{I}\right)_1 I_1 + \left(\frac{V}{I}\right)_2 I_2}{I_1 + I_2}. \tag{3}$$

For the averaging we have checked that the effect of the different barycentric corrections for multiple observations of the same object is much smaller than our spectral resolution. The averaging helps to extract signal hidden in the noise of the individual exposures if the stellar Zeeman signal remains unchanged with time.

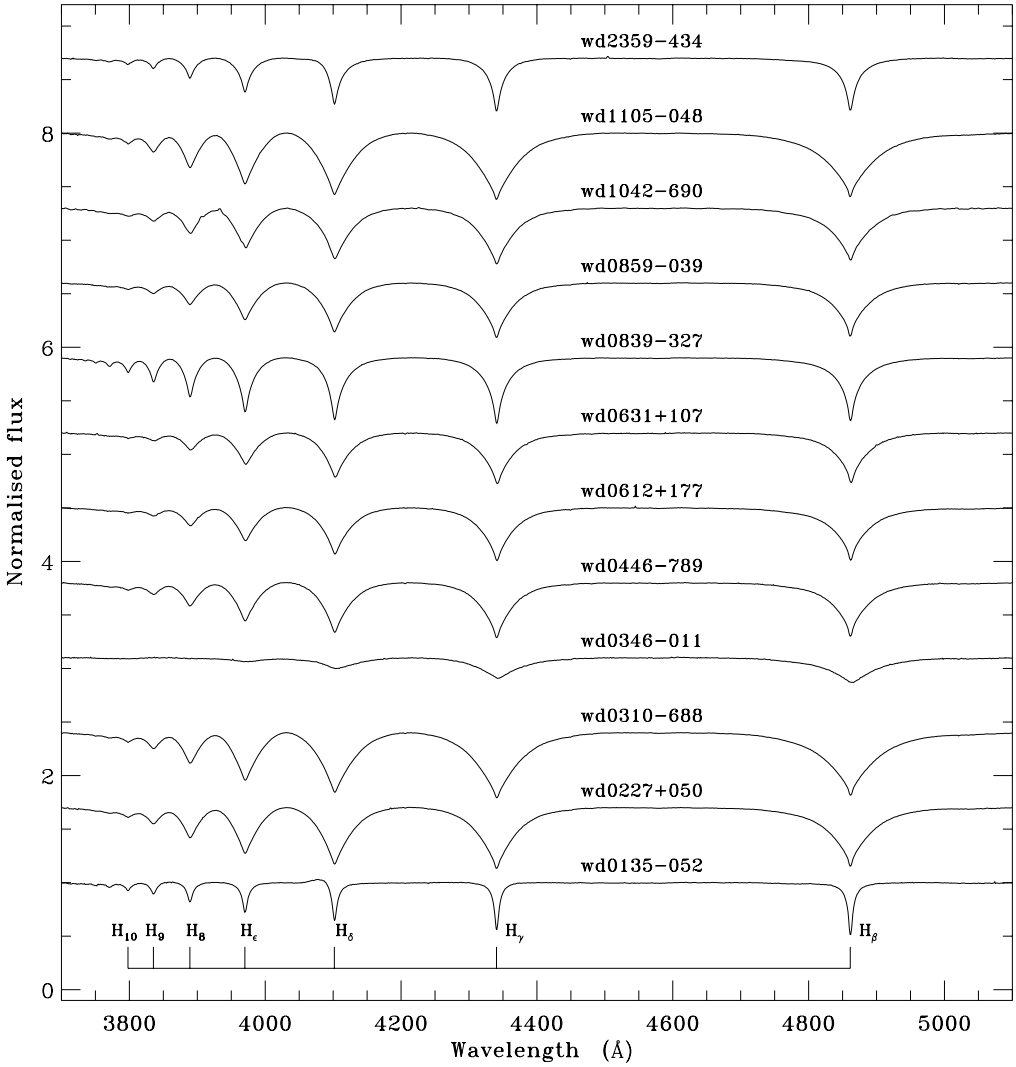

Fig. 1. Normalised spectra of our sample of white dwarfs in the region of the Balmer series. When more than one sequence of exposures was available for a white dwarf, the average spectrum is presented. The positions of the Balmer lines are indicated. The spectra are displaced vertically by 0.7 units (or multiples thereof) for a better visualisation.

Figure 2 shows the circular polarisation spectra (V/I) of our sample of white dwarfs in the region of the Balmer series (no binning along the spectrum was applied to the data). The positions of the Balmer lines are indicated by vertical dashed lines. In two of the averaged spectra (corresponding to stars WD 0446−789 and WD 2359−434) a moderate S-shape circular polarisation signature across Hβ and Hγ can be noticed. For WD 1105−048 polarisation reversals of those lines were only present in the observation of 9 Jan. 2003 (see Fig. 5).

To determine the longitudinal component of the magnetic field for each measurement we compared the observed circular polarisation for an interval of ±20 Å around Hβ and Hγ with the prediction of Eq. (2). The best fit for $\langle B_z \rangle$, the only free parameter, was found by a χ^2-minimisation procedure. If we assume that no magnetic field is present, all deviations from zero polarization are due to noise. This can be expressed by the standard deviation σ over the respective intervals around the Balmer lines. If the best fit magnetic field is indeed close to zero, the reduced χ^2 should be automatically close to unity. However, in the case of a finite magnetic field not all deviations from zero would be due to noise, so that the best fit would have a reduced χ^2 smaller than 1. Following Press et al. (1986) we determined the statistical error from the rms deviation of the observed circular polarisation from the best-fit model. The 1σ (68.3%) confidence range for a degree of freedom of 1 is the interval of B_z where the deviation from the minimum is $\Delta\chi^2 = 1$. Note that this is a purely statistical error and does not account for systematic errors, e.g. from the limitation of our low-field approximation which, however, we expect to be rather small, or from wavelength calibration errors.

The results for each of our single observations is summarized in Table 2, where we have listed the best fits for B_z for the Hβ and Hγ lines as well as the weighted value $B_z = (B_{z,\gamma} w_\gamma + B_{z,\beta} w_\beta)/(w_\gamma + w_\beta)$ where $w_i = 1/\sigma_i^2$ ($i = \gamma, \beta$). The probable error is given by $\sigma = (\sum w_i)^{-1/2}$. When multiple observations were added up to reduce the noise level (by means of Eq. (3)), results are labeled as AVERAGE.

In three stars we find a significant magnetic field: WD 0446−789 (4283 ± 640 G, see Fig. 3), WD 2359−434 (−3138 ± 422 G, see Fig. 4), and WD 1105−048

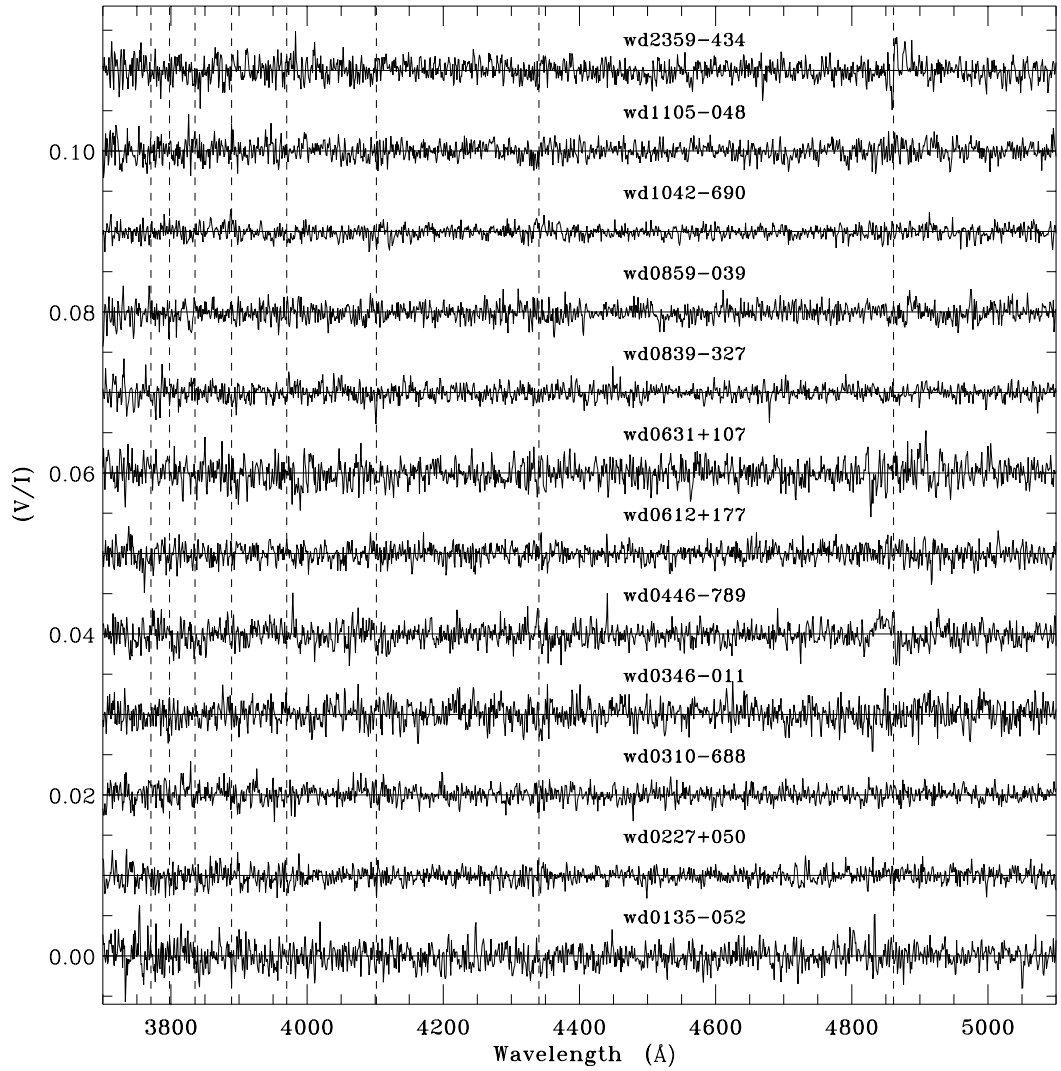

Fig. 2. Circular polarisation spectra (V/I) of our sample of white dwarfs in the region of the Balmer series. The average (V/I)-spectrum is plotted for multiple observations. For all spectra a horizontal line is drawn to indicate the zero level. Dashed vertical lines represent the positions where the Balmer lines are located. Spectra are displaced with relative shifts for a better visualisation.

(-2134 ± 447 G). Positive and negative signs of B_z indicate opposite magnetic polarity. For the first two stars the magnetic field is detected at the 3σ level individually from Hβ and Hγ (at least for the averaged spectra), as well as from the combination of both lines. This increases our confidence in both detections (cf. Sect. 4.3).

Although several lines of the Balmer series are available, the higher members of the series do not contain enough V-signal to give reliable results. However, the analysis of Hδ (the only line among the higher members with its V-signal exceeding the $1\sigma(V)$), confirms the positive detections of magnetic fields in the three objects WD 0446−789, WD 1105−048 and WD 2359−434.

In WD 0446−789 the analysis of the 30 Nov. 2002 observation around Hγ yields a magnetic field of 417 ± 1403 G, corresponding to a $\chi^2_{\rm min} = 1.0$ (instead of $\chi^2_{\rm min} = 0.6$ for the 28 Jan. 2003 observation), i.e. a 0.1σ level detection. If we do not use this outlier for our combined result from the two observations, we obtain a 3σ detection of 4743 ± 832 G.

In the case of WD 1105−048 the different values of the magnetic field obtained for the two observations on 1 Jan. 2003 (-693 ± 497 G) and 29 Jan. 2003 (-3959 ± 710 G, see Fig. 5) differ significantly. This may indicate a different orientation of the magnetic field between the two epochs due to stellar rotation.

The case of WD 0135−052, where the formal value for the combined result from Hβ and Hγ exceeds the 1σ error by a factor of two, is rather uncertain since it is based on one observation only. In addition, this object is a double-lined binary with a period of 1.556 days and it is not clear whether the orbital variation can mimic a magnetic field. This could just be a 2σ level detection, which can be expected for our sample size of field measurements by chance. However, WD 0135−052 is a good candidate for follow-up observations, although one must bear in mind that the magnetic field would be diluted by the presence of a non-magnetic companion.

In all other stars in our sample the best-fit magnetic field is below or close to the 1σ error. In Figs. 3 to 6 the observed circular polarisation spectra of the white dwarfs (thin solid line)

Table 2. Magnetic fields derived from the Hγ and Hβ lines for our sample of white dwarfs. $B(\sigma)$ provides the magnetic field in units of the σ level. Detections exceeding the 3σ levels are given in bold. $\sigma(V)$ is the standard deviation of the observed (V/I)-spectrum obtained in the region 4500–4700 Å. Lower limits on the detectability of the magnetic field from the line polarisation peaks, calculated at the 1σ level of the noise, are given in the last two columns. Multiple observations that were averaged prior to analysis are labeled AVERAGE.

Target	Date	$\sigma(V)$	B(G)		B(G)	$B(\sigma)$	B(G) at 1σ	
		($10^{-3} I_c$)	Hγ	Hβ	Hγ,β	Hγ,β	Hγ	Hβ
WD 0135−052	29/11/02	1.2	1112 ± 625	492 ± 373	654 ± 320	2.04	1277	861
WD 0227+050	28/12/02	1.0	493 ± 1177	−776 ± 707	−439 ± 606	0.72	2486	−1928
	29/01/03	1.0	−710 ± 971	1854 ± 709	962 ± 572	1.68	−2969	1989
	AVERAGE	0.7	−105 ± 789	590 ± 469	408 ± 403	1.01	−1924	1194
WD 0310−688	24/02/03	0.8	−504 ± 741	114 ± 548	−104 ± 440	0.24	−2106	1404
WD 0346−011	28/12/02	1.8	−9299 ± 8510	−6815 ± 5295	−7508 ± 4495	1.67	−36860	−16600
	03/02/03	2.6	3222 ± 9374	7542 ± 6717	6076 ± 5459	1.11	28440	24820
	AVERAGE	1.1	−5967 ± 7087	−1496 ± 4226	−2668 ± 3629	0.74	−23060	−10680
WD 0446−789	30/11/02	1.3	417 ± 1403	4251 ± 910	**3115 ± 763**	4.08	3731	2340
	28/01/03	1.4	7771 ± 1476	5370 ± 1196	**6321 ± 929**	6.80	4118	2815
	AVERAGE	0.9	3612 ± 1005	4743 ± 832	**4283 ± 640**	6.69	2495	1594
WD 0612+177	30/11/02	1.3	2416 ± 1456	−1148 ± 1203	297 ± 927	0.32	4060	−2620
	01/02/03	1.4	86 ± 1154	236 ± 1171	156 ± 821	0.19	3742	2915
	AVERAGE	0.9	1132 ± 920	−457 ± 789	216 ± 598	0.36	2672	−1939
WD 0631+107	01/03/03	2.2	−1310 ± 1785	−170 ± 1815	−749 ± 1272	0.59	−7300	−5890
	03/03/03	2.1	−790 ± 1870	310 ± 1775	−211 ± 1287	0.16	−6630	4340
	AVERAGE	1.2	−990 ± 1440	260 ± 1090	−195 ± 869	0.22	−4010	2630
WD 0839−327	29/11/02	0.7	−313 ± 325	402 ± 261	121 ± 203	0.60	−1008	761
WD 0859−039	03/02/03	1.5	2083 ± 1164	11 ± 987	877 ± 752	1.17	4400	2727
	25/02/03	1.2	2183 ± 1372	−401 ± 911	389 ± 758	0.51	3234	−2222
	AVERAGE	0.8	1186 ± 928	382 ± 607	622 ± 507	1.23	2319	1511
WD 1042−690	28/01/03	1.3	−719 ± 2333	−2850 ± 2301	−1799 ± 1638	1.10	−3624	−3247
	03/02/03	1.0	1627 ± 1464	−865 ± 1163	99 ± 910	0.11	2963	−3560
	24/02/03	0.9	−2374 ± 1060	103 ± 864	−885 ± 669	1.32	−2764	1804
	AVERAGE	0.6	141 ± 745	−406 ± 620	−182 ± 476	0.38	1833	−1508
WD 1105−048	01/01/03	1.1	−1153 ± 632	55 ± 807	−693 ± 497	1.39	−2863	1599
	29/01/03	1.1	−4686 ± 1032	−3305 ± 979	**−3959 ± 710**	5.58	−2756	−2164
	AVERAGE	0.8	−2760 ± 598	−1337 ± 675	**−2134 ± 447**	4.77	−2156	−1538
WD 2359−434	04/11/02	1.0	−3003 ± 1433	−5719 ± 1289	**−4504 ± 958**	4.70	−2914	−2975
	29/11/02	1.0	−1905 ± 702	−4224 ± 796	**−2919 ± 526**	5.55	−4880	−3907
	AVERAGE	1.0	−2066 ± 546	−4738 ± 667	**−3138 ± 422**	7.44	−1785	−1532

are presented together with the (V/I) spectra predicted by the low-field approximation (thick solid line, red colour in the electronic version) for the given value of B. The light shading (cyan in the electronic version) shows the values of (V/I) obtained varying B by the indicated errors, and can be more clearly distinguished from the predicted (V/I) spectra at the peaks of the S-wave features (in particular in the region of Hγ).

4.3. Accuracy of the fitting procedure

Although the χ^2 fitting provides formal errors, it is difficult to judge whether this error actually provides a reasonable estimate of the confidence range for our purpose. For example, the choice of our interval of ±20 Å around Hβ and Hγ is arbitrary. Therefore, we performed simulations for different magnetic fields, interval sizes, and noise levels in order to test our approach. The Gaussian noise for our simulated polarisation spectra was provided by the random number generator implemented in IDL.

As an example we used the solution for the average of both WD 0446−789 observations ($B = 4283 \pm 640$ G), its noise level ($\sigma = 0.001$ at both Hβ and Hγ) and calculated 1000 simulated polarisation spectra for the interval size of ±20 Å. The average result for the magnetic field was: 4301 ± 442 G (solution for Hγ,β), 4276±554 G (for Hβ only), and 4339 ± 725 G (for Hγ only). The mean value of B agrees very well with the prescribed value. The mean of the individual standard deviations of the 1000 runs are 413 G, 541 G and 667 G, for Hγ,β, Hβ and Hγ, respectively. This is slightly smaller than 640 G, 832 G and 1005 G from the WD 0446−789 observation. This may be due to the fact that we assume a homogeneous magnetic field which may not be the case in reality, or it may indicate a small hidden source of errors in the data (e.g. a non-Gaussian distribution of the noise).

Figure 6 shows one of the artificial polarisation measurements from our 1000 simulations. The fit is 4449 ± 449 G in this particular example. It demonstrates that a highly significant detection is possible at our noise level.

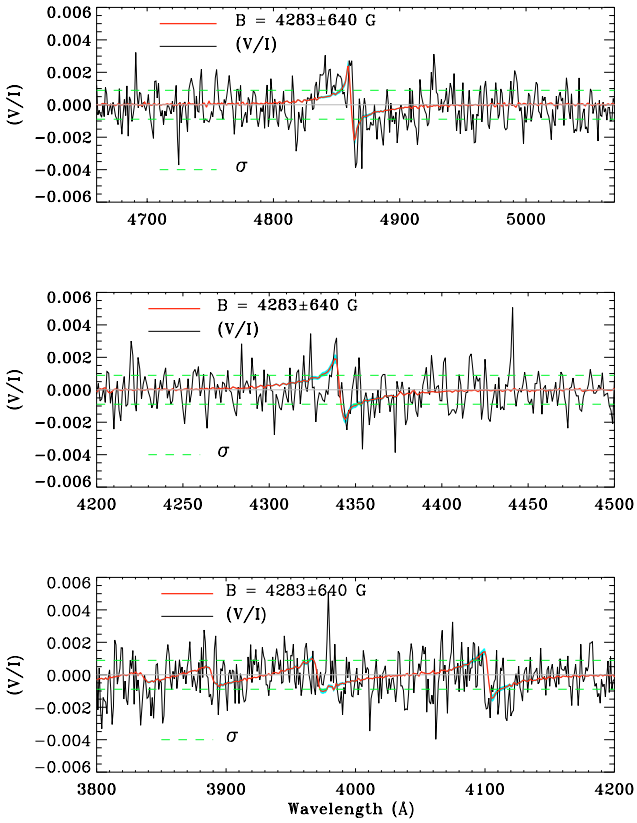

Fig. 3. Circular polarisation spectra (V/I) of WD 0446−789 (average of observations from 30/11/03 and 28/01/03, thin solid line) in the region of Hβ (*top*), Hγ (*middle*) and close to the Balmer jump (*bottom panel*). The solid horizontal line indicates the zero level. The horizonal dashed lines indicate the position of the 1σ level of the average (V/I) spectrum. The light shading (cyan in the electronic version) represents the variation between (V/I) spectra predicted by the low-field approximation (Eq. (2)) using magnetic field values of 4283 ± 640 G (thick solid line, red in the electronic version).

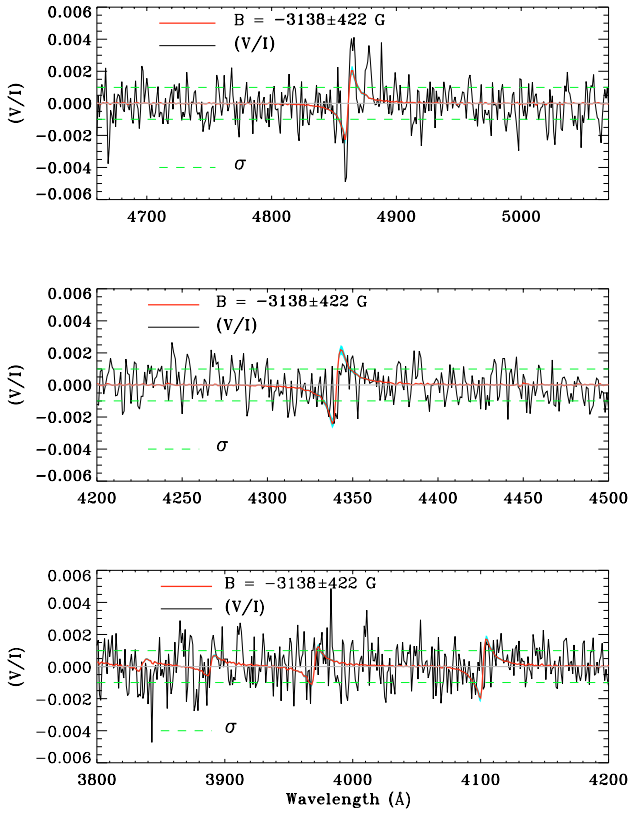

Fig. 4. As in Fig. 3 but for WD 2359−434 (average of observations from 04/11/03 and 29/11/03), where the best fit is at $\langle B_z \rangle$ = −3138 ± 422 G.

The resulting magnetic field changed by less than 2% if an interval of ±40 Å around Hβ and Hγ was used. In the case of a smaller interval, however, larger deviations occur since not the whole range where the predicted (V/I) differs from zero is included.

We are aware of the fact that the polarisation feature is mostly buried in noise in the (V/I)-spectrum, with the exception of the narrow peaks on both sides of the hydrogen line centers. Therefore, on a plot the magnetic information is, to a large extent, invisible to the eye since in the wings the solution is based on an average small excess of right- and left-handed polarisation on different side of the line core, respectively, which clearly contributes to our χ^2 analysis. However, if one wants to obtain an idea of what magnetic field is needed so that the predicted polarisation peaks exceed the 1σ level of the noise, we provide lower limits for this detectability in Cols. 8 and 9 of Table 2. The σ was obtained as the standard deviation of the observed (V/I)-spectrum in a region with no lines over 200 Å (i.e. 4500–4700 Å), for each single observation.

We note that in the three objects (WD 0446−789, WD 1105−048 and WD 2359−434) with a positive detection according to the χ^2 analysis, the peaks of the

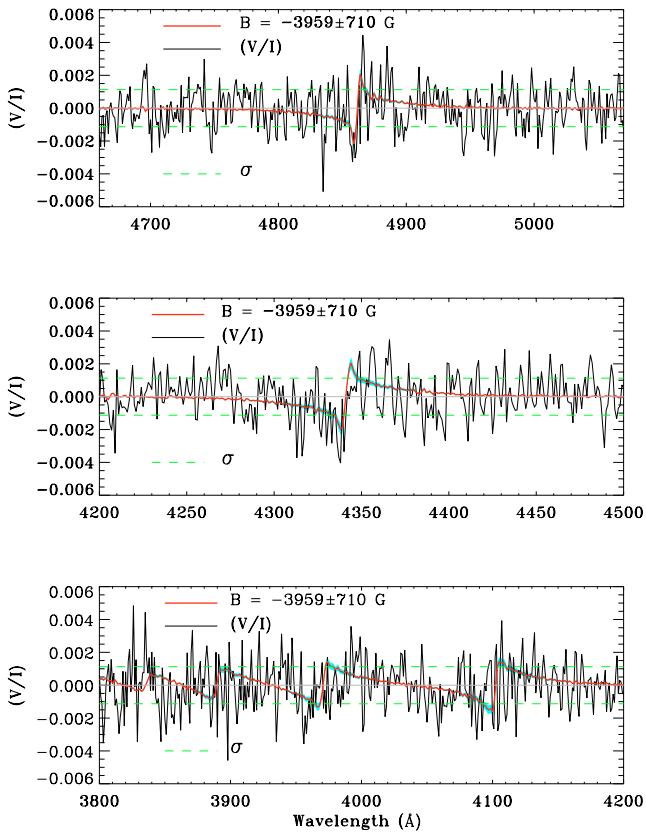

Fig. 5. As in Fig. 3 but for the 09/01/03 observation of the white dwarf WD 1105−048 where the best fit is at $\langle B_z \rangle$ = −3959 ± 710 G.

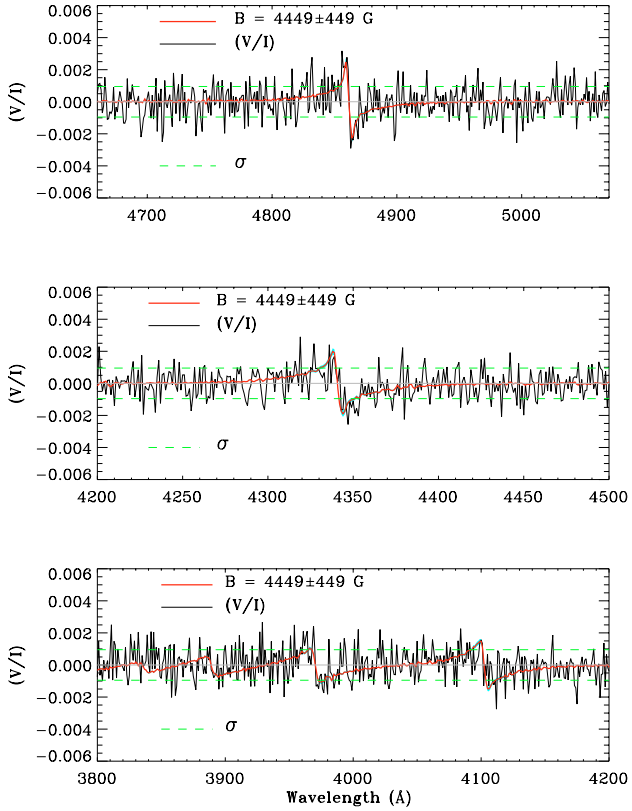

Fig. 6. Artificial polarisation spectrum with the same noise level as WD 0446–789 plotted in Fig. 3. For this particular example, out of the 1000 simulations, the fitting procedure results in $\langle B_z \rangle = 4449 \pm 449$ G.

S-wave circular polarisation signature reaches the 2σ level of the noise so the detection is, therefore, confirmed by this very conservative approach. For the averaged spectra of WD 0446−789 and WD 2359−434, the detections derived from the more reliable Hβ line even reach the 3σ level.

5. Atmospheric and stellar parameters for the target stars

For a discussion of the evolutionary status of our white dwarfs with and without detected magnetic fields we need to know the fundamental parameters of our objects. Masses and cooling ages are of special interest to distinguish between the proposed formation scenarios. These quantities can be computed from the fundamental stellar parameters temperature and gravity, which can be derived by a model atmosphere analysis of the spectra, and theoretical cooling tracks.

Since all white dwarfs selected for our project are bright by white dwarf standards, at least one model atmosphere analysis was published for each object. This is a somewhat inhomogeneous collection of data relying on spectra of different quality and a variaty of methods, including analysis of UV spectra and parallax measurements. Most of the programme stars have already been observed with the SPY project. Although our spectra have lower resolution than the SPY spectra, which aim at the measurement of radial velocity variations seen in the NLTE core of Hα, our flux spectra have a very high signal-to-noise ratio, allowing a very accurate determination of the effective temperatures and gravities.

The observed line profiles are fitted with theoretical spectra from a large grid of NLTE spectra calculated with the NLTE code developed by Werner (1986). Basic assumptions are those of static, plane-parallel atmospheres in hydrostatic and radiative equilibrium. The adopted chemical composition is pure hydrogen, which is appropriate for the stars of our sample. A description of the model calculations and the adopted atomic physics is given in Napiwotzki et al. (1999), where a discussion of the impact of NLTE on the atmospheres and line profiles of DA white dwarfs is provided as well. The coolest four white dwarfs of our sample (WD 0310−688, WD 0839−327, WD 1105−048 and WD 2359−434) were analysed with a grid of LTE model spectra computed by D. Koester for the analysis of DA white dwarfs. The input physics of these model atmospheres is described in some detail in Finley et al. (1997). LTE models are more reliable below 17 000 K, because the NLTE models do not take into account convection and collision induced absorption by hydrogen quasi-molecules. On the other side, NLTE effects are small at these temperatures (Napiwotzki et al. 1999) and of no relevance for our results.

The line fits were performed with a modified version of the least-squares algorithm of Bergeron et al. (1992) described in Napiwotzki et al. (1999). The observed and theoretical Balmer line profiles are normalised to a linear continuum in a consistent manner. Radial velocity offsets are corrected by shifting the spectra to a common wavelength scale. The synthetic spectra are convolved to the resolution of the observed spectra (4.5 Å) with a Gaussian and interpolated to the actual parameters. The atmospheric parameters are then determined by minimising the χ^2 value by means of a Levenberg-Marquardt steepest descent algorithm (Press et al. 1986). This procedure is applied simultaneously to all Balmer lines of one observed spectrum. Formal errors can be derived from the covariance matrix. However, due to the very high signal-to-noise ratios of our spectra, the estimated statistical errors are extremely small (not larger than 20 K in temperature and 0.005 dex in the log of gravity) and do not provide realistic estimates for the whole error budget. The real external errors for the white dwarfs investigated in this article can be estimated to be 2.3% in $T_{\rm eff}$ and 0.07 dex in $\log g$ (Napiwotzki et al. 1999).

Our fit results are provided in columns two and three of Table 3. The parameters are the average of the fit results for the individual spectra. For the reasons discussed above, we do not give the formal fit errors. WD 0135−052 was not fitted by us, because this is a well known double-lined binary consisting of two DA stars (Saffer et al. 1988), which requires a special treatment. White dwarf masses were computed from a comparison of parameters derived from the fit with the grid of white dwarf cooling sequences of Benvenuto & Althaus (1999) for an envelope hydrogen mass of $10^{-4} M_{\rm WD}$, and are given in column four of Table 3. A sample fit is shown in Fig. 7. Most Balmer lines are fitted very well, but the observed profile of Hδ is only poorly reproduced. This results from the reflex in the FORS1 optics mentioned in Sect. 2. Thus we excluded this line from our fitting procedure. However, parameter changes are small, if Hδ is included anyway. Spectroscopic distances d(spec) are

Table 3. Fitted parameters of the white dwarfs and supplementary data from literature. The three objects with positive detections of magnetic fields are labelled in bold face.

WD	$T_{\rm eff}$ (k K)	log g	M ($M_\odot$)	d(spec) (pc)	$t_{\rm cool}$ (Myr)	Literature $T_{\rm eff}$ (k K)	log g	$v \sin i$ (km s^{-1})	d(trig) (pc)
0135−052			0.47/0.52[1,14]			7.47/6.92	7.80/7.89[1,14]		12.3 ± 0.4Y[15]
0227+050	18.45	7.79	0.51	26.1	65	19.07	7.78[2]		24.3 ± 2.9H[16]
						18.21	7.95[16]		
0310−688	15.73	8.00	0.61	11.2	170	15.71	8.16[16]	0±4[10]	10.2 ± 0.2H[16]
						16.18	8.06[4]		
0346−011	43.17	9.08	1.24	34.0	59	39.51	9.07[12]	≤50[17]	
						43.20	9.21[18]		
						40.54	9.22[2]		
						43.10	9.09[4]		
0446−789	23.45	7.72	0.49	48.8	21	23.20	7.70[17]		
						23.61	7.83[4]		
0612+177	25.58	7.86	0.56	46.1	17	24.66	7.94[2]		36.1 ± 2.9Y[15]
						25.17	7.83[5]		
						25.94	7.97[4]		
0631+107	27.25	7.81	0.54	61.9	13	26.59	7.82[5]		
						27.20	8.00[8]		
0839−327	9.24	7.90	0.54	8.3	660	8.80[7]			8.9 ± 0.8Y[15]
						8.93	7.70[3]		
						9.39	7.96[4]		
0859−039	23.78	7.77	0.51	29.1	21	23.22	7.84[12]		
						24.20	7.88[18]		
1042−690	21.42	7.78	0.51	36.3	33	20.64	7.73[6]		
						21.38	7.86[4]		
1105−048	15.28	7.83	0.52	24.5	142	15.58	7.81[4]	<32[13]	
						15.54	7.82[2]		
						15.87[7]			
2359−434	8.66	8.56*	0.95	–	2200	7.76[7]		≈0[10]	7.8 ± 0.4Y[15]
						8.72	8.58[4]		
						8.85	8.57[9]		
						8.67	8.83[11]		

References: [1]Bergeron et al. (1989); [2]Bergeron et al. (1992); [3]Bergeron et al. (2001); [4]Bragaglia et al. (1995); [5]Finley et al. (1997); [6]Kawka et al. (2000); [7]Kepler & Nelan (1993); [8]Kidder et al. (1992); [9]Koester & Allard (1993); [10]Koester et al. (1998); [11]Koester et al. (2001); [12]Napiwotzki et al. (1999); [13]Pilachowski & Milkey (1984); [14]Saffer et al. (1988); [15]van Altena et al. (1995); [16]Vauclair et al. (1997); [17]Vennes (1999); [18]Vennes et al. (1997).

* Gravity fixed at a value which reproduced the absolute brightness computed from the parallax.

determined from the absolute magnitudes computed for the given stellar parameters using the synthetic V band fluxes computed by Bergeron et al. (1995) and the measured V magnitudes given in our Table 1, and are provided in column five of Table 3. Note that the error limits for $T_{\rm eff}$ and log g given above correspond to a 7% error in the distance.

Table 3 is supplemented by physical parameters of our sample of white dwarfs collected from the literature. Fundamental parameters such as temperature and gravity determined by previous spectroscopic studies are given in columns six and seven. The agreement is generally good. Differences are usually within the error limits discussed above. Rotational velocities $v \sin i$, if available, are shown in column eight. If parallax measurements exist, the resulting distances d(trig) are given in column nine (H indicates Hipparcos values, while Y are ground based data from the Yale general catalogue of trigonometric parallaxes).

5.1. Comments on individual objects

WD 0135−052 (L 870−2): We have only one observation of this target, which indicates a very weak magnetic field of 650 G on a 2σ level (see Sect. 4.2). It is reported as a double-lined spectroscopic binary composed of a detached pair of DA white

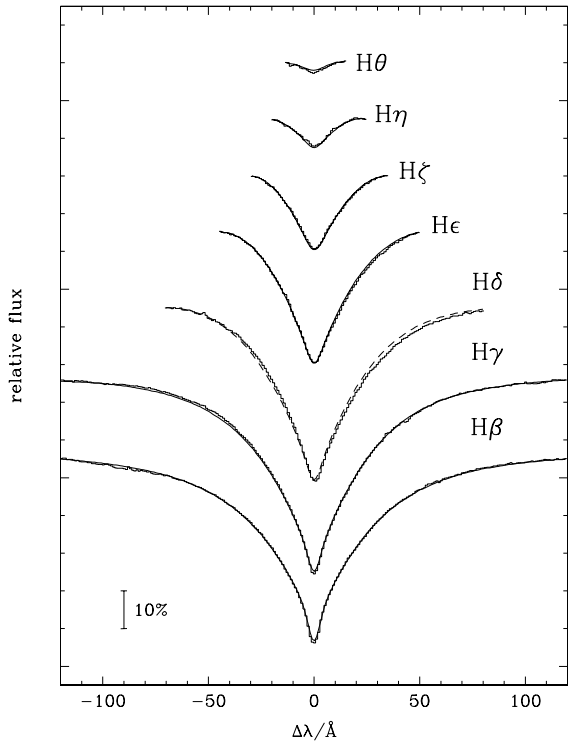

Fig. 7. Model atmosphere fit (solid line) of the 30/11/02 observation of WD 0446−789 (solid histogram). The dashed model profile for Hδ indicates that this line was not used during the fitting procedure.

dwarfs with an orbital period of the system of 1.556 days (Saffer et al. 1988). The system has a mass ratio $q = M_1/M_2 = 0.90$ (Saffer et al. 1988; Bergeron et al. 1989), i.e. the brighter component is less massive. The luminosity ratio of both white dwarfs amounts to 1.5.

WD 0346−011 (GD 50): Bragaglia et al. (1990) list this white dwarf as a suspected double degenerate from their radial velocity measurements. However, the more accurate radial velocity measurements performed by Maxted et al. (2000) and from the SPY spectra indicate a constant radial velocity. GD 50 is a very massive white dwarf ($M = 1.24\ M_\odot$). However, our spectropolarimetric measurements did not detect a significant magnetic field. In our sample, this is the star with the broadest Balmer lines and, consequently, the weakest limit on the magnetic field strength.

WD 0446−789: We found a magnetic field of 4280 G in this relatively young white dwarf (cooling age of 21 Myr) with a mass ($0.49\ M_\odot$) slightly lower than the peak of the white dwarf mass distribution. Maxted et al. (2000) and our SPY observations show that the radial velocity of this star is constant and thus membership in a close binary system can be ruled out.

WD 0612+177 (LTT 11818): By the time a star reaches ∼45 000 K the process of H accumulation has progressed to the point that all white dwarfs are DA in appearance and no DB white dwarfs are observed in the range 30 000–45 000 K, the so-called "DB Gap". WD 0612+177 lies near the red edge of the DB Gap (Holberg et al. 1990), where the onset of near surface convection can mix He into the photospheres of those stars having the thinnest H layers. Holberg et al. (1990) reported the detection of a weak feature due to He I λ4471 in three high signal-to-noise spectra of this white dwarf. From the observed strength of these features those authors obtained estimates of a homogeneous He/H ratio of $\log(\mathrm{He/H}) = -2.56 \pm 0.26$ or, alternatively, a stratified H envelope mass of $\log(M_\mathrm{H}/M_\odot) \sim -16.6 \pm 0.3$. However, subsequent optical observations of this WD by Kidder et al. (1992) did not reveal the 4471 Å features at the strength of the earlier observations. We also do not detect this feature in our two single observations of this WD. One possible explanation given by Kidder et al. is that photospheric He may not be distributed uniformly over the surface of WD 0612+177, possibly due to the presence of a magnetic field and a slow stellar rotation which leads to a modulation of the He I line strengths. Our observations suggest a 3σ upper limit of the magnetic field of less than 2 kG from two different observing dates. This rather tight upper limit needs to be taken into account when considering scenarios to produce a non-uniform distribution of He and H in the white dwarf atmosphere.

WD 0839−327: The quality of our spectral fit is poor compared to other stars in our sample. Our result is virtually identical to the value derived by Bragaglia et al. (1995) using the same technique. Bergeron et al. (2001) using optical and infrared broadband photometry combined with a trigonometric parallax derived lower temperature and gravity. This might indicate that this object is an unresolved binary, consisting of two white dwarfs. This white dwarf is reported as a double degenerate binary by Bragaglia et al. (1990). However, the more accurate measurements done for the SPY project indicate a constant radial velocity ruling out a very close system.

WD 1042−690: This white dwarf has an M type companion in a 0.34 days orbit (Kawka et al. 2000). Some contamination by line emission from the cool companion (mainly Balmer lines and Ca H+K) is present in our spectrum. The contaminated parts of the line profiles were excluded from our fits. Broadband linear polarization could be measureable for this binary due to irradiation and reflection effects. This should, however, not affect our measurement of the circular polarization in spectral lines.

WD 1105−048: For this target we have discovered in the second of two observations the spectropolarimetric signatures from a magnetic field of −3900 G. WD 1105−048 resides in a common proper motion binary with a dM5 companion separated by 279″, corresponding to 6840 AU (Oswalt et al. 1988). The mass of this white dwarf ($0.52\ M_\odot$) is very close to the peak of the white dwarf mass distribution.

WD 2359−434 (L 870−2): For WD 2359−434 we have detected a magnetic field of −3100 G. Already Koester et al. (1998) reported a very shallow and narrow core of the Hα profile observed in this object. They speculated that what they see is only the unshifted component of a Zeeman triplet, with the other components shifted outside the observed spectral range or smeared out due to the inhomogeneity of the field. In favour of this speculation is the unusually high surface gravity of this object, since magnetic white dwarfs tend to be more massive than non-magnetic objects (Liebert 1988). However, it would require a magnetic field >50 kG to shift the σ components outside the spectral range of the Koester et al. observation. No further components could be detected in our spectra or the SPY spectra.

We noticed during the fitting process that our FORS data show flat Balmer lines cores. Available UVES spectra of this white dwarf show that the core of Hα is also flat (as already reported by Koester et al. 1998). Since an accurate parallax measurement exists for WD 2359−434, we modified our fitting procedure for this object. The gravity was fixed at a value, which reproduced the absolute brightness of the white dwarf computed from the parallax. The temperature was determined from a fit of the line wings of the Balmer lines, excluding the cores. Since the absolute brightness depends on the stellar temperature as well, a few iterations were necessary, before we got a self-consistent solution. The derived temperature (8.66 kK) is consistent with the result of Koester & Allard (1993), who fitted UV spectra taken with IUE. Kepler & Nelan (1993) using the same technique, derived a lower temperature (7.76 kK). This is possibly caused by the low value of the surface gravity ($\log g = 8.0$) adopted during their fitting procedure, which is much lower than plausible values for WD 2359−434.

The reason for the flat Balmer line cores of WD 2359−434 remains a mystery. Being a white dwarf with a broad range of magnetic fields is a possible explanation since it would smear out the sigma components. However, in our polarization measurements there is no indication for such a broad range.

6. Discussion and conclusions

In this work we have used the spectropolarimetric capability of the FORS1 instrument, together with the light collecting power of the VLT, to investigate the presence of magnetic fields in the range 1−10 kG for a sample of 12 white dwarfs. Three of the stars out of 12 normal DA white dwarfs of our sample, WD 0446-789, WD 1105-048 and WD 2359-434, exhibit magnetic fields of a few kilogauss in one or all available observations (see Figs. 3–5). The detection rate of 25% suggests strongly that a substantial fraction of white dwarfs have a weak magnetic field.

With the exception of the bright white dwarf 40 Eri B, for which a magnetic field of only 4 kG had been detected (Fabrika et al. 2003), WD 0446−789, WD 1105−048 and WD 2359−434 have the weakest magnetic fields detected so far in white dwarfs. In previous extended searches for weak fields in white dwarfs (e.g. Schmidt & Smith 1995) only very few objects have been found. Only six detections have been reported for magnetic fields below 100 kG, which are not all confirmed, and only three objects have a field weaker than about 50 kG. Kawka et al. (2003) have reported longitudinal magnetic fields in three stars but no significant detection was made because their 1σ error was almost as large as the observed value itself. They concluded that the population of white dwarfs with magnetic fields in excess of 1 MG is well known, but that lower-field white dwarfs remained undetected.

Note, however, that our investigation is based on the averaged longitudinal component of the magnetic field, meaning that the maximum magnetic field at the white dwarf surface can be stronger, depending on the field geometry (described e.g. by offset dipoles, or more complex distributions; with the underestimate being larger for a more complex magnetic distribution) and on the orientation relative to the observer. Therefore, our results for the three objects with a positive detection are lower limits, since cancellation effects are expected.

The population of known magnetic white dwarfs presently comprises some 125 stars (Wickramasinghe & Ferrario 2000; Gänsicke et al. 2002; Schmidt et al. 2003). Wickramasinghe & Ferrario (2000) and Jordan (2001) established that about 3% of all white dwarfs had a magnetic field above 100 kG. Results from the first two years of the Sloan Digital Sky Survey (Gänsicke et al. 2002; Schmidt et al. 2003) show the total number of known magnetic white dwarfs with $B \geq 1.5$ MG being 6%. Recently, Liebert et al. (2003) have found that the incidence of magnetism at the level of ∼2 MG or greater is at least ∼10%, or higher. They suggest that the total fraction of magnetic WDs may be substantially higher than 10% due to the limited spectropolarimetric analyses capable of detecting lower field strengths down to ∼10 kG. Our 3 detections out of 12 objects seem to indicate that low magnetic fields on white dwarfs (<10 kG) are frequent while high magnetic fields are relatively rare. However, with only three detections this hypothesis remains insecure. If confirmed by future observations, the investigation of weak magnetic fields in white dwarfs could form a cornerstone for the future investigation of the properties and evolution of stellar magnetic fields.

Our sample of white dwarfs is too small to discuss in detail the dependence of the magnetic field strength on the stellar parameters (masses and cooling ages). However, two of our detections (WD 0446−789 and WD 1105−048) have masses of only 0.5 $M_{\odot}$. This means that their progenitors on the main-sequence had less than 1 $M_{\odot}$ (Weidemann 2000). These two stars are therefore very different from the majority of white dwarfs with megagauss magnetic fields which tend to have higher masses (Greenstein & Oke 1982; Liebert 1988) and, therefore, high-mass parent stars.

Measurements of weak magnetic fields are now possible for many white dwarfs with the new large telescopes, which allow a magnetic field function (MFF, in analogy to the mass function) to be constructed in the 1−100 kG range once a sufficient number of detections have been made. Such a MFF can be compared to the corresponding function for main-sequence stars (Bychkov et al. 1997) and will provide input for answers to the following key questions on the evolution of magnetic fields in stars: Are the magnetic fields in white dwarfs just the fossil relics of magnetic main-sequence stars strengthened by contraction due to conservation (to a large extent) of magnetic

flux? Or do the magnetic fields develop considerably through the final stages of stellar evolution? Are the strongly magnetic white dwarfs a distinct class of objects or do they represent a tail of the distribution of magnetic fields present in all white dwarfs? Is there a dependence between magnetic field strength and mass as found in the case of magnetic WDs with higher field strengths? Do the magnetic field strengths correlate with temperature, which would be a hint for a decay on the white dwarf cooling sequence?

Several authors have suggested that the frequency of magnetic white dwarfs may increase with decreasing effective temperature, luminosity and with increasing cooling age (e.g. Valyavin & Fabrika 1998; Liebert et al. 2003), and may decrease sharply with distance (Fabrika & Valyavin 1998).

Alternatively to the fossil origin of the magnetic field in white dwarfs, Markiel et al. (1994) and Thomas et al. (1995) have shown that a weak magnetic field of ≈1.3 kG in the variable DB star GD 358 can be explained by an $\alpha\omega$ dynamo. The magnetic field in this star has been inferred indirectly by analyzing the g-mode oscillation spectrum taken with the WET (Whole Earth Telescope, Winget et al. 1994). However, according to the atmospheric parameters, the convection zone in all of our sample stars should be too shallow to support an $\alpha\omega$ dynamo.

Another long-standing problem in white dwarf research is the issue of why metals are accreted by helium-rich white dwarfs in the range 8000 K $< T_{\rm eff} <$ 15 000 K during the passage through an interstellar cloud while almost no hydrogen is brought into the white dwarf atmosphere. Illarionov & Sunyaev (1975) suggested that fields below 10^5 G provide a screening mechanism to separate hydrogen and ionized species from grains in white dwarfs accreting from the interstellar matter. Since this phenomenon always occurs in this type of star, it is possible that at this level all white dwarfs contain magnetic fields. Friedrich et al. (2004) have searched for circular polarisation in one DBZ and one DBAZ which have accreted metals, but three or four orders of magnitude less hydrogen than expected. In one case (L745-46A) a magnetic field of 7 kG (1 σ error of ±2 kG; 99% confidence interval of ±6 kG) was found, which, however, was based on the Hα line only. For the second object (GD 40), only an upper limit of 12 kG (99% confidence) could be derived from polarization measurements around three spectral lines. Theoretically, magnetic fields of 4 kG and 250 kG, respectively, would be required for the screening by the propeller mechanism to be efficient around the two stars.

At our signal-to-noise ratio, magnetic fields down to about 2 kG can be measured. There is still the possibility that all magnetic white dwarfs contain surface magnetic fields at the 1 kG level. To test this hypothesis, much longer exposure times would be necessary, even with the VLT.

Acknowledgements. We gratefully acknowledge useful comments on the effective Landé factor by E. Landi degl'Innocenti. We acknowledge the use of LTE model spectra computed by D. Koester. We thank the staff of the ESO VLT for carrying out the service observations. Work on magnetic white dwarfs in Tübingen is supported by the DLR grant 50 OR 0201. R.N. acknowledges support by a PPARC Advanced Fellowship. We would like to thank the referee J. D. Landstreet for valuable suggestions.

References

Angel, J. R. P., & Landstreet, J. D. 1970, ApJ, 160, L147
Appenzeller, I., Fricke, K., Fürtig, W., et al.1998, ESO-Messenger, 94, 1
Babcock, H. W. 1947, ApJ, 105, 105
Babcock, H. W. 1958, ApJS, 3, 141
Bagnulo, S., Szeifert, T., Wade, G. A., Landstreet, J. D., & Mathys, G. 2001, A&A, 389, 191
Bagnulo, S., Hensberge, H., Landstreet, J. D., Szeifert, T., & Wade, G. A. 2004, A&A, 416, 1149
Benvenuto, O. G., & Althaus, L. G. 1999, MNRAS, 303, 30
Bergeron, P., Wesemael, F., & Beauchamp, A. 1995, PASP, 107, 1047
Bergeron, P., Leggett, S. K., & Ruiz, M. T. 2001, ApJS, 133, 413
Bergeron, P., Saffer, R. A., & Liebert, J. 1992, ApJ, 394, 228
Bergeron, P., Wesemael, F., Fontaine, G., & Liebert, J. 1989, ApJ, 345, L91
Beuermann, K., & Reinsch, K. 2002, A&A, 381, 487
Bragaglia, A., Greggio, L., Renzini, A., & D'Odorico, S. 1990, ApJ, 365, L13
Bragaglia, A., Renzini, A., & Bergeron, P. 1995, ApJ, 443, 735
Bychkov, V. D., Monin, D. N., Fabrika, S. N., & Valyavin, G. G. 1997, in Stellar Magnetic Fields, ed. Y. Glagolevskij, & I. Romanyuk, Proceedings of the International Conference (Special Astrophysical Observatory Press), 124
Casini, R., & Landi degl'Innocenti, E. 1994, A&A, 291, 668
Donati, J. -F., Semel, M., Carter, B. D., Rees, D. E., & Cameron, A. C. 1997, MNRAS, 291, 658
Fabrika, S. N., & Valyavin, G. G. 1998, Bull. Special Astrophys. Obs., 45, 84
Fabrika, S. N., Valyavin, G. G., & Burlakova, T. E. 2003, Astron. Lett., 29, 737
Finley, D. S., Koester, D., & Basri, G. 1997, ApJ, 488, 375
Friedrich, S., Jordan, S., & Koester, D. 2004, A&A, submitted
Gänsicke, B. T., Euchner, F., & Jordan, S. 2002, A&A, 394, 957
Greenstein, J. L., & Oke, J. B. 1982, ApJ, 252, 285
Hagen, H.-J., Groote, D., Engels, D., et al. 1987, A&A, 183, L7
Holberg, J. B., Kidder, K. M., & Wesemael, F. 1990, ApJ, 365, L77
Illarionov, A. F., & Sunyaev, R. A. 1975, A&A, 39, 185
Jordan, S. 2001, in 12th European Workshop on White Dwarfs, ed. J. L. Provencal, et al., ASP Conf. Ser., 226, 269
Jordan, S., & Friedrich, S. 2002, A&A, 383, 519
Kawka, A., Vennes, S., Dupuis, J., & Koch, R. 2000, AJ, 120, 3250
Kawka, A., Vennes, S., Wickramasinghe, D. T., Schmidt, G. D., & Koch, R. 2003, in White Dwarfs, ed. D. de Martino, et al., Kluwer Academic Publishers. NATO Science Series II, 105, 179
Kemp, J. C., Swedlund, J. B., Landstreet, J. D., & Angel, J. R. P. 1970, ApJ, 161, L77
Kepler, S. O., & Nelan, E. P. 1993, AJ, 105, 608
Kidder, K. M., Holberg, J. B., Barstow, M. A., Tweedy, R. W., & Wesemael, F. 1992, ApJ, 394, 288
Koester, D., & Allard, N. F. 1993, in White Dwarfs: Advances in Observation and Theory, ed. M. A. Barstow (Dordrecht: Kluwer), 237
Koester, D., Dreizler, S., Weidemann, V., & Allard, N. F. 1998, A&A, 338, 612
Koester, D., Napiwotzki, R., Christlieb, N., et al. 2001, A&A, 378, 556

Landi degl'Innocenti, E., & Landi degl'Innocenti, M. 1973, Sol. Phys., 29, 287
Landstreet, J. D. 1982, ApJ, 258, 639
Liebert, J. 1988, PASP, 100, 1302
Liebert, J., Bergeron, P., & Holberg, J. B. 2003, AJ, 125, 348
Markiel, J. A., Thomas, J. J., & Van Horn, H. M. 1994, ApJ, 430, 834
Mathys, G. 2001, Magnetic Fields Across the Hertzsprung-Russell Diagram, ed. G. Mathys, et al., ASP Conf. Ser., 248, 267
Maxted, P. F. K., Marsh, T. R., & Moran, C. K. J. 2000, MNRAS, 319, 305
McCook, G. P., & Sion, E. M. 1999, ApJS, 121, 1
Mestel, L. 2001, Magnetic Fields Across the Hertzsprung-Russell Diagram, ed. G. Mathys, et al., ASP Conf. Ser., 248, 3
Napiwotzki, R., Christlieb, N., Drechsel, H., et al. 2001, AN, 322, 411
Napiwotzki, R., Christlieb, N., Drechsel, H., et al. 2003, ESO-Messenger, 112, 25
Napiwotzki, R., Green, P. J., & Saffer, R. A. 1999, ApJ, 517, 399
Neiner, C., Geers, V. C., Henrichs, H. F., et al. 2003a, A&A, 406, 1019
Neiner, C., Hubert, A.-M., Frémat, Y., et al. 2003b, A&A, 409, 275
Oswalt, T. D., Hintzen, P. M., & Luyten, W. J. 1988, ApJS, 66, 391
Pilachowski, C. A., & Milkey, R. W. 1984, PASP, 96, 821
Press, W. H., Flannery, B. P., & Teukolsky, S. A. 1986, Numerical Recipes (Cambridge: Univ. Press)
Putney, A. 1995, ApJ, 451, L67
Reimers, D., Jordan, S., Koehler, T., & Wisotzki, L. 1994, A&A, 285, 995
Rüedi, I., Solanki, S. K., Mathys, G., & Saar, S. H. 1997, A&A, 318, 429
Saar, S. H. 1996, in IAU Coll., 153, Magnetodynamic Phenomena in the Solar Atmosphere – Prototypes of Stellar Magnetic Activity, ed. Y. Uchida, et al. (Dordrecht: Kluwer), 367
Saffer, R. A., Liebert, J., & Olszewski, E. W. 1988, ApJ, 334, 947
Schmid, H. M., Appenzeller, I., & Burch, U. 2003, A&A, 404, 505
Schmidt, G. D., Harris, H. C., Liebert, J., et al. 2003, ApJ, 595, 1101
Schmidt, G. D., & Smith, P. S. 1994, ApJ, 423, L63
Schmidt, G. D., & Smith, P. S. 1995, ApJ, 448, 305
Szeifert, T., & Böhnhardt, J. D. 2003, FORS1+2 User Manual 2.6; ESO document VLT-MAN-ESO-13100-1543
Thomas, J. H., Markiel, A., & Van Horn, H. M. 1995, ApJ, 453, 403
Tinbergen, J., & Rutten, R. 1997, Measuring polarisation with ISIS, Users' manual, The Isaac Newton Group of Telescopes
Valenti, J. A., & Johns-Krull, C. 2001, Magnetic Fields Across the Hertzsprung-Russell Diagram, ed. G. Mathys, et al., ASP Conf. Ser., 248, 179
Valyavin, G. G., & Fabrika, S. N. 1998, Bull. Special Astrophys. Obs., 45, 69
van Altena, W. F., Lee, J. T., & Hoffleit, E. D. 1995, The general catalogue of trigonometric parallaxes, 4th ed. (New Haven: Yale University Observatory)
Vauclair, G., Schmidt, H., Koester, D., & Allard, N. 1997, A&A, 325, 1055
Vennes, S. 1999, ApJ, 525, 995
Vennes, S., Thejll, P., Génova-Galvan, R., & Dupuis, J. 1997, ApJ, 480, 714
Weidemann, V. 2000, A&A, 363, 647
Werner, K. 1986, A&A, 161, 177
Wickramasinghe, D. T., & Ferrario, L. 2000, PASP, 112, 873
Winget, D. E., Nather, R. E., Clemens, J. C., et al. 1994, ApJ, 430, 839
Wolff, B., Jordan, S., & Koester, D. 1996, A&A, 307, 149